A Riemannian Framework for Intrinsic Comparison of Closed Genus-Zero Shapes

Boris A. Gutman[1,2(✉)], P. Thomas Fletcher[3], M. Jorge Cardoso[2], Greg M. Fleishman[1], Marco Lorenzi[2], Paul M. Thompson[1], and Sebastien Ourselin[2]

[1] Imaging Genetics Center, INI, University of Southern California, Los Angeles, USA
bgutman@gmail.com
[2] Center for Medical Image Computing, University College London, London, UK
[3] School of Computing, University of Utah, Salt Lake City, USA

Abstract. We present a framework for intrinsic comparison of surface metric structures and curvatures. This work parallels the work of Kurtek et al. on parameterization-invariant comparison of genus zero shapes. Here, instead of comparing the embedding of spherically parameterized surfaces in space, we focus on the first fundamental form. To ensure that the distance on spherical metric tensor fields is invariant to parameterization, we apply the conjugation-invariant metric arising from the L^2 norm on symmetric positive definite matrices. As a reparameterization changes the metric tensor by a congruent Jacobian transform, this metric perfectly suits our purpose. The result is an intrinsic comparison of shape metric structure that does not depend on the specifics of a spherical mapping. Further, when restricted to tensors of fixed volume form, the manifold of metric tensor fields and its quotient of the group of unitary diffeomorphisms becomes a proper metric manifold that is geodesically complete. Exploiting this fact, and augmenting the metric with analogous metrics on curvatures, we derive a complete Riemannian framework for shape comparison and reconstruction. A by-product of our framework is a near-isometric and curvature-preserving mapping between surfaces. The correspondence is optimized using the fast spherical fluid algorithm. We validate our framework using several subcortical boundary surface models from the ADNI dataset.

Keywords: Shape analysis · Riemannian metric · Surface registration · Cortical surface

1 Introduction

Analysis of surfaces plays an important role in medical image processing. Surfaces representing boundaries of functionally and structurally distinct regions, such as the cortex and subcortical structures, can be locally analyzed and compared in lieu of full volumetric analysis. Succinct and easily visualized, such a representation offers tremendous power for morphometric analysis. However, the non-Euclidean nature of surface geometry significantly complicates this approach compared to volume-based methods.

S. Ourselin et al. (Eds.): IPMI 2015, LNCS 9123, pp. 205–218, 2015.
DOI: 10.1007/978-3-319-19992-4_16

A number of computational tools for surface analysis have been developed. Gu et al., developed a conformal mapping algorithm [1] for spherical mapping and formulated a landmark-matching energy as a Mobius transform. A relaxation of the conformal energy, the quasi-conformal mapping of Zeng et al. [2] simultaneously solves the Beltrami equations and minimizes curvature mismatch. Shi et al. [3] applies fluid registration to the flat 2D domain after conformally mapping a surface with prescribed boundaries. Spherical Demons [4], a less straightforward adaptation of a Euclidean registration algorithm, applies the diffeomorphic demons algorithm [5] to the sphere, matching curvature-derived intensity functions to match sulcal patterns of the cortex. A similar approach is taken [6], adapting fluid registration [7] to the sphere. Yet another family of algorithms computes high-dimensional embeddings of surfaces based on eigenfunctions of the Laplace-Beltrami operator [8]. This elegant approach locally adapts the metric tensor by scaling in order to more closely match the embeddings of two surfaces in the Euclidean sense.

Many of these methods produce reasonable and often quite good results for a wide range of problems. The "missing link" in much of the work above is the restriction of the problem to registration. Once the surfaces are registered it is not generally possible to know how one of the surfaces may develop to become the other, or how further deformation in the same direction may look. Comparison of surfaces is out of sync with the spatial alignment procedure, either using local setting-specific features, such as cortical thickness or radial distance, or applying deformation-based analysis after the registration step. An example the latter is surface Tensor-Based Morphometry (shape TBM) [9]. With this in mind, it is clear that a framework unifying surface registration, comparison, and reconstruction is ultimately desired.

In some sense, the "holy grail" of morphometric analysis of any kind that addresses the issue above is the development of a Riemannian manifold with non-vanishing geodesics. Developing the appropriate Riemannian metric for one's object of interest, such as curves, surfaces, or deformation fields, immediately allows the application of various tools from the Riemannian machinery. Examples of these tools include computing manifold statistics, geodesic shooting and parallel transport of velocities for predicting longitudinal change, etc. [10–12]. Well-known examples of Riemannian manifold structures in medical imaging have been developed for the space of diffeomorphisms (LDDMM) [13], curves in $\mathbb{R}^n$ [14], as well as surface embeddings [15, 16] and diffusion tensors [12]. Reference [17] applies the large deformation framework to compute distances between surfaces as the length of the path in the space of diffeomorphism resulting from morphing one boundary onto another. An improvement on this is suggested in [15], measuring distances on the deformation of the surface itself rather than in the ambient space as done in [17]. Closer still to our work here, Kurtek et al. [16] developed a Riemannian framework for surfaces of spherical topology, using "q-map" representation. The L^2 distance on q-maps, or simply the surface embedding locally weighted by the square root of the volume form, is shown to be invariant under spherical automorphisms. From this, a definition of a path length is developed, encapsulating the degree of spatial deformation between surfaces up to rotation and spherical remapping of one surface over the other. A path-straightening algorithm explicitly parameterized in time is then implemented, allowing both geodesic computation and interpolation. The beauty of this Riemannian approach lies in the ability to

directly reconstruct the surface from the representation, which is not found in the surface-based methods discussed above. However, the representation is still of the surface *embedding*, with all the resulting nuisances. To overcome this, some standard heuristics are applied to the initial surfaces, namely centering each shape at the origin. Thus, a local change in the surface has a global effect on the representation. More importantly, the approach applies to the space $\mathcal{S}$ of smooth functions from the 2-sphere to $\mathbb{R}^n$, without any regard for the intrinsic metric structure of the surface. One undesirable effect of this is that the resulting geodesics may enter regions of $\mathcal{S}$ corresponding to surfaces with unrealistically severe metric distortion.

Hoping to avoid these confounds, we instead begin with the notion of intrinsic surface representation that is already invariant to nuisance parameters such as Euclidean motion, while capturing the metric structure. Our ultimate goal is a metric space on a complete surface representation. By "complete," we mean a representation from which a surface can be reconstructed uniquely up to initialization parameters. In general, the ability to reconstruct the object from the representation is not guaranteed, as some of the examples of Riemannian settings above show.

A basic result from surface geometry, the Fundamental Theorem of Surfaces states that a surface can be uniquely represented up to Euclidean motion with two smooth symmetric tensor fields satisfying certain integrability. With the additional constraint that the first of the tensor fields is positive definite, a surface can be reconstructed given an initial frame. The first of these fields is the Riemannian metric tensor on the surface g_{ij}, while the second is the Second Fundamental Form II, or "shape tensor." In this work, we mainly focus on the metric tensor. To develop a distance on metric tensors of surfaces, we turn to the work of Ebin [18] and others [19, 20] who have developed a Riemannian framework for the general manifold of metrics tensors. Applying the results to our case – pullback metrics on the 2-sphere induced from the mapped surfaces – we develop a parameterization-invariant comparison of surface metric structures. We show how this measure can be extended to be a metric, when the metric tensor space is restricted to a sub-manifold of fixed-form metrics. Augmenting this distance with metrics on curvatures, we develop a complete representation for surfaces of spherical topology. We apply our method to several brain structures. We show that our method leads to an equiareal mapping between surfaces that is as-conformal-as-possible.

2 A Riemannian Metric on the Space of Metric Tensors

Given an n-dimensional manifold M, the space of all smooth symmetric tensor fields $\Sigma(M) = \{h : TM \times TM \to \mathbb{R} | h \,\varepsilon\, Sym(n)\}$ and the subspace of Σ of positive definite tensors $\mathcal{M}(M) = \{h : TM \times TM \to \mathbb{R} | h \in SPD(n)\}$, our problem above can be restated generally as finding a suitable metric on $\mathcal{M}$, such that the group of diffeomorphisms on M acts on $\mathcal{M}$ by isometry. Ebin et al. [18] showed that the L^2 Riemannian metric on the tangent bundle of $\mathcal{M}$, each fiber of which is identified with Σ, indeed satisfies this criteria: given $g \in \mathcal{M}, h, k \in \Sigma \cong T_g\mathcal{M}$, the metric can be written as:

$$(h,k)_g = \int_M \langle h,k\rangle_g d\mu_g, \tag{1}$$

where $\langle h,k\rangle_g$ is the inner product induced by g, $\langle h,k\rangle_g = tr(g^{-1}hg^{-1}k)$, and μ_g is the volume form also induced by g. This metric produces geodesics on $\mathcal{M}$ whose length can be computed point-wise and in closed form. In other words, a geodesic on $\mathcal{M}$ is a one-parameter family of metrics g_t on M, with the tensor at a point $x \in M$, $g(x)$ depending only on $g_0(x)$ and $g_0'(x)$. Applying these results to our concrete case, we take M to be the 2-sphere $\mathbb{S}^2$, and consider the space of metrics pulled back from spherically parameterized surfaces $\mathcal{S} = \left\{S : \mathbb{S}^2 \to \mathbb{R}^3 | S \in C^\infty\right\}$, expressed in canonical coordinates on $T\mathbb{S}^2$ as $g_{i,j} = S_i^T S_j$. We illustrate an example of this representation in Fig. 1. A reparameterization $\varphi \in \Phi = \left\{\phi : \mathbb{S}^2 \to \mathbb{S}^2 \middle| \phi, \phi^{-1} \in C^2\right\}$ acts on g by conjugation with the pushforward (Jacobian) $D\varphi : T_x\mathbb{S}^2 \to T_{\varphi(x)}\mathbb{S}^2$, $\varphi \circ g = D\varphi^T g D\varphi$. Given two parameterized surfaces $A, B \in \mathcal{S}$, a closed-form solution for the geodesic distance between g_A and g_B at a point x is [21]

$$D(g_A[x], g_B[x]) = \sqrt{\int_0^1 \left\langle g_t'(x), g_t'(x)\right\rangle_{g_{t(x)}} dt} = \left\| \mathrm{Log}\left[g_A^{-1/2} g_B g_A^{-1/2}\right] \right\|_F. \tag{2}$$

This metric is indeed invariant under simultaneous spherical re-mappings of A and B, since $D(g_A, g_B) = D(D\varphi^T g_A D\varphi, D\varphi^T g_B D\varphi)$. These results are derived in [21].

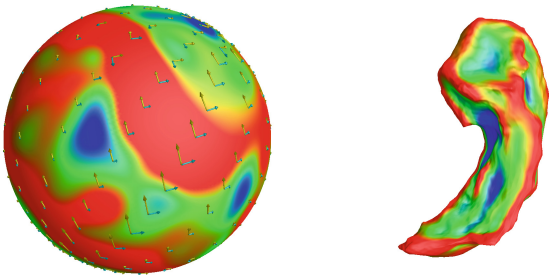

Fig. 1. Metric tensor fields and mean curvature – a nearly complete surface representation. Tensors are displayed as their eigenvectors in $T\mathbb{S}^2$ with magnitude corresponding to the eigenvalues. If Gaussian curvature (not shown) is also known, the information on the left is sufficient to reconstruct the hippocampal surface on the right.

3 Parameterization-Invariant Metric Tensor Comparison

While the measure above is pointwise-invariant to conjugation, integrating the expression following (1) does not in fact le to a measure that is invariant. This is due to the changing volume form in (1). As we will see, a trade-off must be made between three desirable properties of a shape comparison measure: **1.** Invariance under actions

by Φ; **2.** Point-wise independence; **3.** Metric property. Only two of these three properties can be satisfied simultaneously on $\mathcal{M}$. The first of these is crucial for intrinsic shape comparison, for if it fails to hold, the measure is subject to the arbitrary nature of an initial spherical parameterization. The third property can be useful for all the reasons described in the introduction, such as computing intrinsic means and transporting trajectories. The second property is attractive for the ease of computation it implies: the problem reduces to minimizing the integral of the pointwise measures over M. For now, we choose to preserve the first two properties. This requires us to modify the volume form on $\mathbb{S}^2$ to be symmetric with respect to A and B, and independent of the spherical mapping. We define our measure as

$$P(A,B) = \int_{\mathbb{S}^2} \left\| \mathrm{Log}\left[g_A^{-1/2} g_B g_A^{-1/2} \right] \right\|_F^2 [det(g_A) det(g_B)]^{1/4} d\mathbb{S}^2 \tag{3}$$

The volume form $[det(g_A)det(g_B)]^{1/4}d\mathbb{S}^2$ remains unchanged after a re-mapping $\left[det\left(g_A^{\varphi}\right)det\left(g_B^{\varphi}\right)\right]^{1/4}df(\mathbb{S}^2) = [det(g_A)det(g_B)]^{1/4}\det(D\varphi)d\mathbb{S}^2 \det(D\varphi^{-1}) = [det(g_A)$ $det(g_B)]^{1/4}d\mathbb{S}^2$. Together with the result from the previous section, this shows that $P(\varphi \circ A, \varphi \circ B) = P(A,B)$. Finding the global minimum of P by re-parameterizing one surface over the other, we obtain a comparison between the two surfaces' metric structures that is independent of parameterization and therefore intrinsic:

$$P^*(A,B) = \min_{\varphi \in \Phi} P(A, \varphi \circ B), A, B \in \mathcal{S}. \tag{4}$$

The measure above is appealing: it leads to a mapping between two surfaces that minimizes metric distortion with a mixture of equiareal and conformal mapping between the surfaces. The minimization reduces to a standard registration problem over spherical automorphisms, with the cost function (3). Further, the mapping between the two surfaces retains its metric-preserving property regardless of the initial spherical mapping: here the sphere is a "dummy space," only needed as a standard canonical space for computational convenience. However, we cannot say that $P^*(A,B)$ is a metric.

4 Metrics on $M_\mu \backslash \Phi_U$ and on the Space of Surfaces

The change in the volume form due to reparameterization prevents a straightforward generalization of $(\cdot,\cdot)_g$. To the quotient space $\mathcal{M}\backslash\Phi$. This is the reason for the breakdown in the metric property of the measure $P^*(A,B)$. However, the submanifold $\mathcal{M}_\mu$ of metrics which correspond to a fixed measure μ admits this generalization. $\mathcal{M}_\mu$ is a metric space under $(\cdot,\cdot)_g$, with the geodesic distance defined as usual: $d(g_A, g_B) = \min_{g_0=g_A, g_1=g_B} \sqrt{\int_0^1 \left(g_t', g_t'\right)_{g_t} dt}$. Taking its quotient by the appropriate restriction of Φ to maps with a unitary pushforward $\Phi_U = \{\phi \in \Phi | det(D\phi) = 1\}$, we see that $\mathcal{M}_\mu \backslash \Phi_U$ is also a metric space under the related metric

$$d^*(g_A, g_B) = \min_{\phi_t \in \{\varphi_t:[0,1]\to\Phi_U\}} d(g_A, \phi_t \circ g_B)$$
$$= \min_{\substack{g_0 = g_A, g_1 = g_B \\ \phi_t \in \{\varphi_t : [0,1] \to \Phi_U\}}} \sqrt{\int_0^1 \left(g_t'(\phi_t), g_t'(\phi_t)\right)_{g_t} dt} \tag{5}$$

Further, it is known that $\mathcal{M}_\mu \backslash \Phi_U$ is geodesically complete [19], i.e. the exponential map is defined on the entire tangent space. In particular, this means that geodesic shooting is possible following transport of any velocity between any pair of points on $\mathcal{M}_\mu \backslash \Phi_U$. The obvious choice for a concrete example of $\mathcal{M}_\mu$ is the set of metrics arising from area-preserving spherical maps, i.e. $\mathcal{S}_m = \{S \in \mathcal{S} | det(g_S) = m\}$ for some constant m. Ensuring scale invariance, we further restrict $\mathcal{S}_m$ to $\mathcal{S}_1$ by rescaling surfaces to have area 4π.

Restricting the space of allowable parameterizations to $\mathcal{S}_1$ may seem like a high price to pay for the ability to use the Riemannian machinery. Yet, it is least restrictive among the three standard parameterizations: conformal, Tuette and equiareal. The genus-zero conformal mapping, for example, only has six degrees of freedom, while the Tuette energy has a unique minimum [1]. The registration arising from this restriction is an equiareal mapping that is as-conformal-as-possible. Thus, we can still expect the resulting registration to approximate near-isometric maps, though perhaps not as well as an unconstrained optimization of $P^*(A, B)$. A generic path between two points g_A, g_B on $\mathcal{M}(\mathcal{S}_1)\backslash\Phi_U$ may be parameterized at a point on $\mathbb{S}^2$ using a family of diffeomorphisms $\phi_t \in \{\varphi_t : [0,1] \to \Phi_U\}$ as

$$g_t(\phi_t) = g_A^{1/2} e^{t\mathrm{Log}\left[g_A^{-1/2} D\phi_t^T (\phi_t \circ g_B) D\phi_t g_A^{-1/2}\right]} g_A^{1/2}.$$

The velocity takes the form

$$g_t'(\phi_t) = g_A^{1/2} \left(\int_0^1 e^{\alpha t S(t)} [S(t) + tS'(t)] e^{(1-\alpha) t S(t)} d\alpha \right) g_A^{1/2},$$

$$S(t) = \mathrm{Log}\left[g_A^{-1/2} D\phi_t^T (\phi_t \circ g_B) D\phi_t g_A^{-1/2} \right].$$

The geodesic path length can then be written as

$$\mathfrak{D}^*(A, B) = d^*(g_A, g_B), A, B \in \mathcal{S}_1$$

In general, the fact that Φ_U acts on $\mathcal{M}_\mu$ by isometry does not imply that ϕ_t is stationary, i.e. $\phi\prime_t \neq 0$ [19]. Nevertheless, this simplifying assumption leads to a far more tractable problem. Indeed, the authors in [16] implicitly make the same assumption. With this simplification at ha, we write our intrinsic metric on the metric structures of genus-zero shapes as

$$\mathfrak{D}(A, B) = \min_{\varphi \in \Phi_U} P(A, \varphi \circ B), A, B \in \mathcal{S}_1 \tag{6}$$

The metric $\mathfrak{D}(A,B)$ allows us to compute intrinsic distances between metric structures of surfaces of spherical topology. Yet, the metric structures alone do not represent surfaces uniquely. As a simple example, an inflated and a deflated tennis ball have zero distance between them on $\{\mathcal{M}(\mathcal{S}_1)\backslash\Phi_U, \mathfrak{D}(\cdot,\cdot)\}$. To achieve a unique representation, curvature information must be invoked. In principle, any surface can be reconstructed locally given an initial coordinate frame, if g and $II = \boldsymbol{n}^T S_{ij}$ are known [22]. The last term is the shape tensor in local coordinates, where $\boldsymbol{n}$ is the surface normal. The reconstruction can be done following two integrations, so long as the Gauss-Codazzi equations are satisfied:

$$\begin{aligned} L_2 - M_1 &= L\Gamma^1_{12} + M\left(\Gamma^2_{12} - \Gamma^1_{11}\right) - N\Gamma^2_{11} \\ -N_1 + M_2 &= L\Gamma^1_{22} + M\left(\Gamma^2_{22} - \Gamma^1_{12}\right) - N\Gamma^2_{12}, \end{aligned} \tag{7}$$

where the shape tensor is expressed explicitly as $II = \begin{pmatrix} L & M \\ M & N \end{pmatrix}$, and Γ^k_{ij} are the Christoffel symbols. Given a global parameterization with spherical boundary conditions, we can derive II using (7) from the mean and Gaussian curvature only, $H = tr(\mathscr{s})/2, K = det(\mathscr{s})$, where the shape operator $\mathscr{s} = IIg^{-1}$. Several approaches are possible, including explicitly solving (7) numerically. A simpler approach [23] solves for the normal curvatures from H, K, and fits $\mathscr{s}$ locally by solving a least squares problem; the shape tensor can then be computed as $II = \mathscr{s}g$. The implication is that we only need to define a distance on two scalar quantities in addition to g. Because H, K are invariant to parameterization, L^2 distances on fields of curvatures on $\mathbb{S}^2$ are trivially invariant to action by Φ_U. We then define our genus-zero shape metric as the 1-product metric on $\mathfrak{S} = \left\{\mathcal{M}(\mathcal{S}_1) \times C^2\left(\mathbb{S}^2\right) \times C^2\left(\mathbb{S}^2\right)\right\}\backslash\Phi_U$,

$$\mathcal{L}(A,B) = \mathfrak{D}(A,B) + D_{L^2\backslash\Phi_U}(H_A, H_B) + D_{L^2\backslash\Phi_U}(K_A, K_B). \tag{8}$$

Here, $C^2\left(\mathbb{S}^2\right) = \left\{f : \mathbb{S}^2 \to \mathbb{R} \middle| f \in C^2\right\}$, and the usual L^2 distance modified by Φ_U, $D_{L^2\backslash\Phi_U}(a,b) = \min_{\phi_t \in \{\varphi_t:[0,1]\to\Phi_U\}} \sqrt{\int_0^1 \int_{\mathbb{S}^2} (a - \phi_t \circ b)^2 d\mathbb{S}^2 dt}$. Given two spherically parameterized surfaces A, B, the geodesic connecting them on $\mathfrak{S}$ can be parameterized explicitly at every point on $\mathbb{S}^2$ as

$$\{g_t, H_t, K_t\} = \{g_t(\phi_t), H_A + t(\phi_t \circ H_B - H_A), K_A + t(\phi_t \circ K_B - K_A)\}, \tag{9}$$

where $\phi_t \in \{\varphi_t : [0,1] \to \Phi_U\}$ is solution of the optimization problem in (8). Here, as before, we make the simplifying assumption that ϕ_t is stationary.

5 Solving for ϕ with Fluid Registration on $\mathbb{S}^2$

We adapt an optimization approach similar to [6]. Briefly, spherical warps are parameterized by tangential vector fields $\boldsymbol{u} : \mathbb{S}^2 \to T\mathbb{S}^2$, with $\varphi[\boldsymbol{u}(x), x] = x\sqrt{1 - \|\boldsymbol{u}(x)\|^2} - \boldsymbol{u}(x)$, with $\boldsymbol{u}, x$ expressed in ambient $\mathbb{R}^3$ coordinates. The length of

the geodesic on $\mathbb{S}^2$ connecting x and $\varphi[\boldsymbol{u}(x), x]$ is the arcsine of $\|\boldsymbol{u}(x)\|$. This parameterization was also used in [4]. The drawback is that warps transferring points more than 90 degrees cannot be modeled. This still allows for very large deformations, while simplifying the computation.

Fluid registration is based on modeling the simplified Navier-Stokes equation $\mu\Delta\boldsymbol{v}(x,t) + (\lambda+\mu)\vec{\nabla}\left(\vec{\nabla}\cdot\boldsymbol{v}(x,t)\right) = -\boldsymbol{F}[\varphi[\boldsymbol{u}(x,t),x]]$. The force field $\boldsymbol{F}$ represents the gradient of the objective function, and λ, μ are Lame coefficients [7]. The time-varying velocity $\boldsymbol{v}$ is integrated explicitly over time to obtain $\boldsymbol{u}$. In [6], the authors use the material derivative to account for the effect of the Jacobian when updating $\boldsymbol{u}$ by the instantaneous velocity: $\frac{\partial \boldsymbol{u}}{\partial t} = [D\varphi]\boldsymbol{v}$, where $\frac{\partial \boldsymbol{u}}{\partial t}$ is expressed in local coordinates in $T_{\varphi(x)}\mathbb{S}^2$. The pushforward $D\varphi$ connecting local frames at x and $\varphi(x)$ can be computed as $D\varphi = \left[\frac{\partial y}{\partial s}, \frac{\partial y}{\partial t}\right]^T_{y=\varphi(x)} \left[\frac{\partial \varphi}{\partial x}\right] \left[\frac{\partial y}{\partial s}, \frac{\partial y}{\partial t}\right]_{y=x}$, where s, t are local coordinates of tangent spaces, and

$$\frac{\partial \varphi}{\partial x} = I\left(1 - \|\boldsymbol{u}\|^2\right)^{1/2} - x\left[\left(\frac{\partial \boldsymbol{u}}{\partial x}\right)\boldsymbol{u}\right]^T \left(1 - \|\boldsymbol{u}\|^2\right)^{-1/2} - \left(\frac{\partial \boldsymbol{u}}{\partial x}\right). \tag{10}$$

Accounting for the non-linearity in the parameterization of φ to update the field $\boldsymbol{u}$ in the Eulerian frame, we must find $\boldsymbol{u}(x, t+\delta t)$ for a small time step δt, so that $\varphi[\boldsymbol{u}(x,t+\delta t),x] = \varphi[\boldsymbol{u}(x,t),x]\sqrt{1 - \left\|\delta t \frac{\partial \boldsymbol{u}}{\partial t}\right\|^2} - \delta t \frac{\partial \boldsymbol{u}}{\partial t}$. This can be done using the cross-product matrix $G(x)$, where $G(x)y = x \times y$, by $\boldsymbol{u}(x, t+\delta t) = G^2\varphi[\boldsymbol{u}(x, t+\delta t), x]$.

We approximate the solution to the Navier-Stokes equation by filtering the force field with a Gaussian kernel, $\boldsymbol{v} \approx -\mathbf{K}_\sigma * \boldsymbol{F}$, which is a solution of the isotropic diffusion equation $\frac{\partial \mathbf{v}}{\partial t} = -\Delta\mathbf{v}, \sigma = \sqrt{2t}$, where Δ is the spherical *vector* Laplacian. This can be solved efficiently with vector spherical harmonics $\mathbf{B}_{lm}, \mathbf{C}_{lm}$, $\mathbf{K}_\sigma * \mathbf{v}(p) = \sum_{\substack{l=1 \\ |m|\le l}}^{\infty} e^{-l(l+1)\sigma}[\mathbf{B}_{lm}\langle\mathbf{B}_{lm}, \mathbf{v}\rangle + \mathbf{C}_{lm}\langle\mathbf{C}_{lm}, \mathbf{v}\rangle]$. See [6] for details.

The force field $\boldsymbol{F}$ coincides with the direction minimizing the cost function corresponding to the shape metric (8):

$$\begin{aligned}\mathcal{C}(A, B, \boldsymbol{u}) = P(A, \varphi[\boldsymbol{u}] \circ B) + \int_{\mathbb{S}^2} (H_A - \varphi[\boldsymbol{u}] \circ H_B)^2 + (K_A - \varphi[\boldsymbol{u}] \circ K_B)^2 d\mathbb{S}^2 \\ + R\int_{\mathbb{S}^2} (\log det[D\varphi[\boldsymbol{u}]])^2 d\mathbb{S}^2\end{aligned} \tag{11}$$

The second term is simply an L^2 minimization problem, whose gradient is well-known. The last term, ensuring that the remapping φ remains in Φ_U, is similar to a regularization term used in 3D image registration [24]. The first term contains the most novelty; here, we derive its Euler-Lagrange equation. In detail,

$$P(A, \varphi[\boldsymbol{u}] \circ B) = \int_{\mathbb{S}^2} L(\varphi[\boldsymbol{u}, x], x) d\mathbb{S}^2, \quad L = \|\mathrm{Log}X(\varphi[\boldsymbol{u}, x], x)\|^2, \tag{12}$$

where $X(\varphi[\boldsymbol{u},x],x) = g_A^{-1/2}(x)D\phi^T(x)g_B(\varphi[\boldsymbol{u},x])D\phi(x)g_A^{-1/2}(x)$. Note that we have dropped the determinant terms, as they remain unchanged under Φ_U. For simplicity, we first derive the E-L equations at $\boldsymbol{u} \equiv 0$. Since $\frac{\partial}{\partial t}\|\mathrm{Log}X(t)^2\| = 2tr\left[\|\mathrm{Log}XX^{-1}\frac{d}{dt}X\|\right]$, [21] the Lagrangian derivative with respect to $\boldsymbol{u}$ is

$$\frac{\partial L}{\partial u^i} = -2tr\left[\mathrm{Log}X\,X^{-1}g_A^{-1/2}\frac{\partial}{\partial x^i}\{g_B(x)\}g_A^{-1/2}\right]. \tag{13}$$

We show the second-order terms for the first coordinate only:

$$\frac{\partial L}{\partial\left(\frac{\partial u^1}{\partial x^1}\right)} = -2tr\left[\mathrm{Log}X\,X^{-1}g_A^{-1/2}\begin{pmatrix} 2g_{B,11} & g_{B,21} \\ g_{B,21} & 0 \end{pmatrix}g_A^{-1/2}\right], \tag{14}$$

$$\frac{\partial L}{\partial\left(\frac{\partial u^1}{\partial x^2}\right)} = -2tr\left[\mathrm{Log}X\,X^{-1}g_A^{-1/2}\begin{pmatrix} 0 & g_{B,11} \\ g_{B,11} & 2g_{B,21} \end{pmatrix}g_A^{-1/2}\right].$$

The expressions for the second coordinate are analogous. The descent direction minimizing $P(A, \varphi[\boldsymbol{u}] \circ B)$ is then

$$F^j = \sum\nolimits_{i=1}^{2}\frac{d}{dx^i}\frac{\partial L}{\partial\left(\frac{\partial u^j}{\partial x^i}\right)} - \frac{\partial L}{\partial u^j}. \tag{15}$$

In fact, estimates at $\boldsymbol{u} \equiv 0$ are sufficient to perform the entire optimization: we only need to transport the metric fields by the current deformation to compute the gradient at an arbitrary $\boldsymbol{u}$ using (13–15).

6 Implementation Details

6.1 Initialization

We initially compute area-preserving spherical maps using Freidel's robust mapping [6]. We then perform all our computations on a regular spherical grid with direct reference to the original triangle meshing of both the parameterization and the original mesh. We maintain a harmonic bandwidth between 64 and 256, which corresponds to roughly between 16 K and 260 K control points. Due to the local nature of fluid registration, we must have a good initialization. We take an approach similar to [6], performing a coarse global search over the space of rotations to match the curvatures.

6.2 Tensor and Curvature Estimation

In order to compute the metric tensors in local spherical coordinates, we fit a quadratic surface at each regular grid point, but using the original meshing. The fitting is done with respect to all the vertices in the 1-ring of faces around the triangle containing the

regular grid point. We then compute g and $\frac{\partial g}{\partial x}$ in local coordinates analytically from the fitted coefficients. At each iteration of the fluid algorithm, the original spherical parameterization of the moving mesh B is brought forward by $p \rightarrow \varphi^{-1}(p)$, and the transformed tensors are computed fresh over the new spherical mesh. We estimate curvatures directly on the original mesh following [23]. Curvature estimates on triangle meshes are notoriously noisy, and we apply mild Laplacian smoothing directly on the original mesh to H and K to obtain reasonable estimates. These are then interpolated onto the regular grid.

6.3 Surface Reconstruction

In Sect. 4, we proposed to reconstruct a surface by first solving for the shape tensor. In practice, we take a more direct approach, solving an auxiliary least squares problem based on discrete differential geometry operators [23]. Given a spherical mesh $m = \langle V, E \rangle$, $|x| = 1 \forall x \in V$, and g, H, K defined at each vertex, the mesh representing an embedding in space, $\langle S(V), E \rangle$ minimizes three least-squares problems:

$$E_g = \sum\nolimits_{x \in V} \boldsymbol{A}(x) \sum\nolimits_{y \in N_1(x)} \left[(Sx - Sy)^2 - (x - y)^T g(x)(x - y) \right]^2,$$

$$E_H = \sum\nolimits_{x \in V} \boldsymbol{A}(x) \left(\left\langle \left[\sum\nolimits_{y \in N_1(x)} \frac{\left(\cot a_{xy} + \cot b_{xy}\right)(Sx - Sy)}{4\boldsymbol{A}(x)} \right], \boldsymbol{n} \right\rangle - H(x) \right)^2,$$

$$E_K = \sum\nolimits_{x \in V} \boldsymbol{A}(x) \left(\frac{2\pi - \left[\sum\nolimits_{y,z \in N_1(x), yz \in E} \cos^{-1} \frac{\langle (Sy - Sx), (Sz - Sx) \rangle}{|(Sy - Sx)||(Sz - Sx)|} \right]}{\boldsymbol{A}(x)} - K(x) \right)^2.$$

Here, $\boldsymbol{n}$ is the surface normal, $\boldsymbol{A}(x)$ is the area element, and a_{xy}, b_{xy} are angles opposite edge xy. On a regular spherical grid, the area element is estimated as $\boldsymbol{A}(x) = \frac{1}{2} det(g)^{\frac{1}{2}} \sin\theta(x) \left(\frac{\pi}{BW}\right)^2$, for bandwidth BW. The initial conditions are set using a single spherical triangle (x, y, z), so that $Sx = 0$, $Sy = \left(\|y - x\|_{g(x)}, 0, 0 \right)$. $Sz = \left(\|z - x\|_{g(x)} \cos\omega, \|z - x\|_{g(x)} \sin\omega, 0 \right)$, $\omega = \cos^{-1} \frac{\langle z - x, y - x \rangle_{g(x)}}{\|z - x\|_{g(x)} \|y - x\|_{g(x)}}$, $\langle p, q \rangle_g = p^T g q$.

7 Experiments

We applied our metric tensor registration to hippocampal and caudate surfaces of 100 Alzheimer's patients (AD) and 100 controls. In addition, we applied our method to a pair of cortical surfaces from different subjects from the same dataset. In all cases, the fluid registration was performed in 3 stages, with the kernel of the vector Gaussian set to $\sigma = 10^{-1}, \sigma = 10^{-2}, \sigma = 10^{-3}$. In general, we found that better overall results are achieved if an additional non-linear registration step is taken before this process, only minimizing curvature mismatch. Overall computation time at $BW = 128$ is on the order of 10 min, requiring 10–100 iterations at each stage.

In the first experiment, we tested the metric-preserving property of our method compared to curvature-only registration. We illustrate with a pair of caudate surfaces in Fig. 2. The angle distortion is far more widespread in the curvature-only case, indicating that the cost function in (11) preserves the metric structure between the two surfaces. Comparing distributions of distortion in hippocampal registration shows the same point. We compared the mean difference between distortion levels of the two registration approaches. Random pairs of subjects' hippocampi were registered, using the entire dataset. Unsurprisingly, the metric distance method lead to significantly lower distortion, $t = -19.9$.

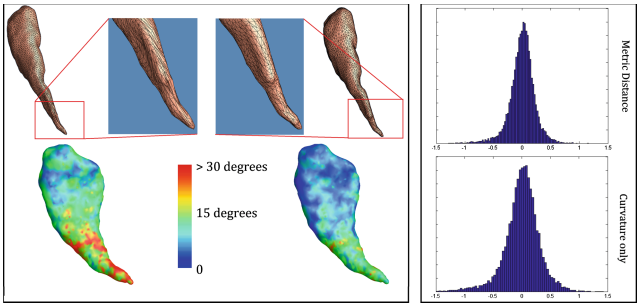

Fig. 2. Left Panel: Metric distortion using only curvature matching (left), and metric tensor registration (right). The top caudate surface is registered to the bottom one. Colors represent absolute angle distortion between the surfaces. **Right Panel:** Distributions of angle distortion in radians for hippocampal surface registration (Color figure online).

To test the reliability of our surface reconstruction method, we computed the geodesics between a surface model of the nucleus accumbens, and a caudate model. While this is certainly not representative of a real application, it is a good test of robustness of our method. Equally reasonable results hold for cortical metric registration. We illustrate the results in Fig. 3.

To examine the usefulness of the shape distance itself, we compared the annual rate of change in hippocampal and caudate shape between AD patients and controls. Shape change was computed as the geodesic length between corresponding surfaces over 1 year. We also made the same comparison using change in hippocampal and caudate volume. Results are displayed in Table 1. It is encouraging to see that shape change in our framework is somewhat more sensitive to disease effects.

Table 1. Rate of change difference between AD and controls: shape and volume.

	Left Hippocampus	Right Hippocampus	Left Caudate	Right Caudate
Shape	$\mathcal{L}_{AD} - \mathcal{L}_{CTL} = 0.81$ $\boldsymbol{P = 0.0002}$	0.92 $\boldsymbol{P < 0.0001}$	0.64 $\boldsymbol{P = 0.0014}$	0.98 $\boldsymbol{P = 0.0007}$
Volume (mm^3)	20.1 $\boldsymbol{P = 0.001}$	23.2 $\boldsymbol{P < 0.0001}$	12.4 $\boldsymbol{P = 0.027}$	11.7 $\boldsymbol{P = 0.003}$

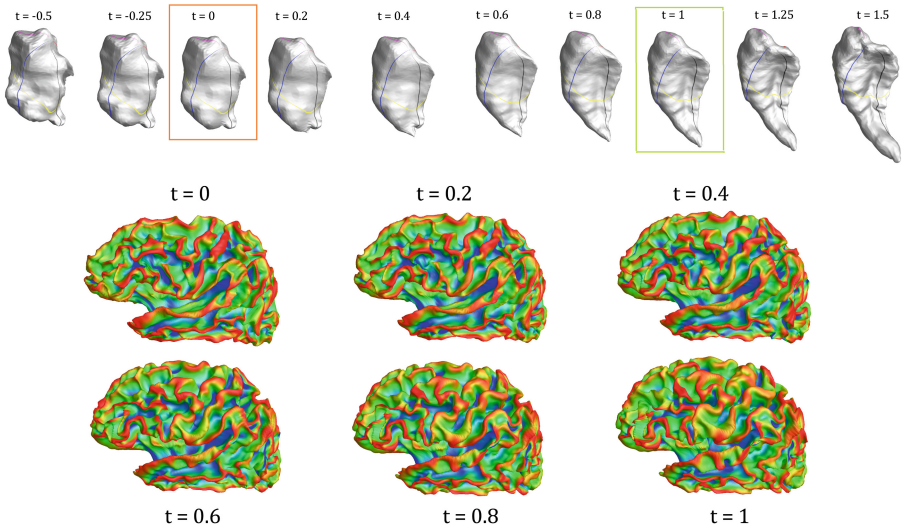

Fig. 3. Top Panel: geodesics between a caudate and a nucleus accumbens models. Extending the path beyond the original end-points continues to generate reasonable reconstructions. Path length $\mathcal{L} = 28.8$ **Bottom Panel:** geodesic between two cortical surfaces. $\mathcal{L} = 11.2$

8 Conclusion

We have presented a Riemannian framework for analyzing metric structures of shapes that are topologically equivalent to the sphere. Our "metric space of metrics" is defined by a conjugation-invariant distance on symmetric (0,2)-tensors. When augmented with metrics on curvature maps, the product space becomes a proper metric space of shapes. Due to computational constraints, we do not optimize our geodesics over the entire set of paths in this space, but restrict the search to paths up to a stationary diffeomorphism. Because our geodesic path lengths can then be computed in closed form, this results in a very efficient algorithm: no path-straightening is required. We show that the geodesic search in our space leads to robust near-isometric and curvature-preserving mapping, with the ability to reconstruct surfaces along the path. Our measure is able to detect disease-related shape change in subcortical structures with greater sensitivity than volume. While we do not consider size and rigid motion in our framework, metrics on affine transformations already exist [25]. These can be joined with the metric presented here for a more complete analysis of objects in space.

References

1. Gu, X., Wang, Y., Chan, T.F., Thompson, P.M., Yau, S.T.: Genus zero surface conformal mapping and its application to brain surface mapping. IEEE Trans. Med. Imaging **23**, 949–958 (2004)

2. Zeng, W., Lui, L.M., Luo, F., Chan, T.F.-C., Yau, S.-T., Gu, D.X.: Computing quasiconformal maps using an auxiliary metric and discrete curvature flow. Numer. Math. **121**, 671–703 (2012)
3. Shi, J., Thompson, P.M., Gutman, B., Wang, Y.: Surface fluid registration of conformal representation: application to detect disease burden and genetic influence on hippocampus. NeuroImage **78**, 111–134 (2013)
4. Yeo, B.T.T., Sabuncu, M.R., Vercauteren, T., Ayache, N., Fischl, B., Golland, P.: Spherical demons: fast diffeomorphic landmark-free surface registration. IEEE Trans. Med Imaging **29**, 650–668 (2010)
5. Vercauteren, T., Pennec, X., Perchant, A., Ayache, N.: Diffeomorphic demons: efficient non-parametric image registration. NeuroImage **45**, S61–S72 (2009)
6. Gutman, B.A., Madsen, S.K., Toga, A.W., Thompson, P.M.: A family of fast spherical registration algorithms for cortical shapes. In: Shen, L., Liu, T., Yap, P.-T., Huang, H., Shen, D., Westin, C-Fk (eds.) MBIA 2013. LNCS, vol. 8159, pp. 246–257. Springer, Heidelberg (2013)
7. Christensen, G.E., Rabbitt, R.D., Miller, M.I.: Deformable templates using large deformation kinematics. IEEE Trans. Med. Imaging **5**, 1435–1447 (1996)
8. Yonggang, S., Rongjie, L., Wang, D.J.J., Pelletier, D., Mohr, D., Sicotte, N., Toga, A.W.: Metric optimization for surface analysis in the Laplace-Beltrami embedding space. IEEE Trans. Med. Imaging **33**, 1447–1463 (2014)
9. Wang, Y., Yuan, L., Shi, J., Greve, A., Ye, J., Toga, A.W., Reiss, A.L., Thompson, P.M.: Applying tensor-based morphometry to parametric surfaces can improve MRI-based disease diagnosis. NeuroImage **74**, 209–230 (2013)
10. Fletcher, P.T., Venkatasubramanian, S., Joshi, S.: The geometric median on Riemannian manifolds with application to robust atlas estimation. NeuroImage **45**, S143–S152 (2009)
11. Joshi, S.H., Joshi, A.A., Gutman, B., Toga, A.W., McMahon, K., De Zubicaray, G., Martin, N., Wright, M.J., Thompson, P.M.: Genetic influences on sulcal patterns of the brain. In: 2012 9th IEEE International Symposium on Biomedical Imaging (ISBI), pp. 414–417 (2012)
12. Fletcher, P.T., Joshi, S.: Riemannian geometry for the statistical analysis of diffusion tensor data. Signal Process. **87**, 250–262 (2007)
13. Miller, M.I., Younes, L.: Group actions, homeomorphisms, and matching: a general framework. Int. J. Comput. Vision **41**, 61–84 (2001)
14. Joshi, S.H., Klassen, E., Srivastava, A., Jermyn, I.: An efficient representation for computing geodesics between n-dimensional elastic shapes. In: Proceedings of IEEE Conference on Computer Vision and Pattern Recognition (2007)
15. Bauer, M., Bruveris, M.: A new Riemannian setting for surface registration. In: 3rd MICCAI Workshop on Mathematical Foundations of Computational Anatomy, pp. 182–194 (2011)
16. Kurtek, S., Klassen, E., Zhaohua, D., Jacobson, S.W., Jacobson, J.B., Avison, M.J., Srivastava, A.: Parameterization-invariant shape comparisons of anatomical surfaces. IEEE Trans. Med. Imaging **30**, 849–858 (2011)
17. Qiu, A., Younes, L., Miller, M.I., Csernansky, J.G.: Parallel transport in diffeomorphisms distinguishes the time-dependent pattern of hippocampal surface deformation due to healthy aging and the dementia of the Alzheimer's type. NeuroImage **40**, 68–76 (2008)
18. Ebin, D.G.: On the space of Riemannian metrics. Bull. Am. Math. Soc. **74**(5), 1001–1003 (1968)
19. Clarke, B.: The metric geometry of the manifold of Riemannian metrics over a closed manifold. Calc. Var. **39**, 533–545 (2010)
20. Bauer, M., Bruveris, M., Michor, P.W.: Overview of the geometries of shape spaces and diffeomorphism groups. J. Math. Imaging Vision **50**, 60–97 (2014)

21. Moakher, M.: A differential geometric approach to the geometric mean of symmetric positive-definite matrices. SIAM J. Matrix Anal. Appl. **26**, 735–747 (2005)
22. Millman, R.S., Parker, G.D.: Elements of Differential Geometry. Prentice-Hall, Englewood Cliffs (1977)
23. Meyer, M., Desbrun, M., Schröder, P., Barr, A.: Discrete differential-geometry operators for triangulated 2-manifolds. In: Hege, H.-C., Polthier, K. (eds.) Visualization and Mathematics III, pp. 35–57. Springer, Heidelberg (2003)
24. Leow, A.D., Yanovsky, I., Chiang, M.C., Lee, A.D., Klunder, A.D., Lu, A., Becker, J.T., Davis, S.W., Toga, A.W., Thompson, P.M.: Statistical properties of Jacobian maps and the realization of unbiased large-deformation nonlinear image registration. IEEE Trans. Med. Imaging **26**, 822–832 (2007)
25. Woods, R.P.: Characterizing volume and surface deformations in an atlas framework: theory, applications, and implementation. NeuroImage **18**(3), 769–788 (2003)